Enhanced Sampling of Configuration and Path Space
in a Generalized Ensemble by Shooting Point Exchange

Sebastian Falkner, Alessandro Coretti, and Christoph Dellago[*]

University of Vienna, Faculty of Physics, 1090 Vienna, Austria

The computer simulation of many molecular processes is complicated by long timescales caused by rare transitions between long-lived states. Here, we propose a new approach to simulate such rare events, which combines transition path sampling with enhanced exploration of configuration space. The method relies on exchange moves between configuration and trajectory space, carried out based on a generalized ensemble. This scheme substantially enhances the efficiency of the transition path sampling simulations, particularly for systems with multiple transition channels, and yields information on thermodynamics, kinetics and reaction coordinates of molecular processes without distorting their dynamics. The method is illustrated using the isomerization of proline in the KPTP tetrapeptide.

Overcoming high free energy barriers to explore configuration and trajectory space in simulations of rare events is at the core of the sampling problem. Numerous enhanced sampling techniques have been developed to address this problem and study the thermodynamics and kinetics of rare events such as nucleation, chemical reactions, and biomolecular reorganization [1–5]. However, when choosing the most suitable method, a conflict of interest arises. Enhanced sampling methods such as metadynamics [6,7] and umbrella sampling [8] efficiently focus computational resources on the regions of interest while still allowing for reweighting to retrieve the equilibrium distribution. However, the dynamics of the system are distorted by the bias potential. In contrast, path sampling methods such as transition path sampling (TPS) and transition interface sampling (TIS) allow us to obtain true-dynamic trajectories between stable states [9,10]. However, these schemes may suffer from correlations between subsequently sampled trajectories, especially for systems with several reaction channels. This problem can be alleviated by applying enhanced sampling methods to path space [11–14]. In addition, points on reactive trajectories are not distributed according to the equilibrium distribution and reweighting samples requires knowledge of the committor probability [15].

In this Letter, we propose a rare event simulation scheme based on sampling configuration and path space in parallel, e.g., using metadynamics and TPS. The two simulations are coupled by exchanging configurations between them following an acceptance criterion derived for a generalized ensemble. As a result, transition paths show less correlations due to fast relaxation in configuration space and barriers in configuration space are crossed more frequently due to exchanges with configurations on transition paths.

Exchange moves, e.g., as employed in replica exchange molecular dynamics [16,17] or replica exchange TIS [18], are a powerful tool to enhance sampling and reduce correlations. In such moves [19], configurations of two systems are exchanged and accepted according to a criterion that ensures a properly weighted ensemble in both systems. Here, we propose to perform exchange moves between a configuration y from a given distribution $p_y(y)$ and a configuration on a path X from the distribution of transition paths $P_X^{AB}[X]$, which includes only paths that connect two given regions A and B. For this purpose, we define a generalized ensemble with joint distribution

$$P_z(z) = p_y(y)P_X^{AB}[X(\tau)], \qquad (1)$$

where the state $z = \{y, X(\tau)\}$ with a configuration y and a path $X(\tau)$ of length τ. The probability density of reactive paths $P_X^{AB}[X(\tau)]$ is given by [10]
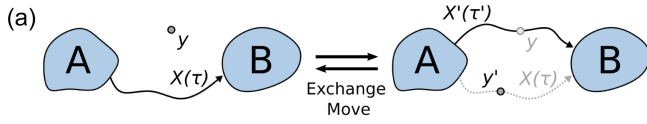
$$P_X^{AB}[X(\tau)] = \frac{1}{Z_{AB}} H_{AB}[X(\tau)]P_X[X(\tau)], \qquad (2)$$

where Z_{AB} is a normalizing factor. The factor $H_{AB}[X(\tau)]$ is unity if the trajectory connects states A and B in any order while having only a single point inside each state. Otherwise, $H_{AB}[X(\tau)]$ is zero. The probability distribution of an unconstrained path, $P_X[X(\tau)]$, is given by [10]

$$P_X[X(\tau)] = p_{eq}(x_0) \prod_{i=0}^{\tau/\Delta t - 1} p(x_{i\Delta t} \to x_{(i+1)\Delta t}), \qquad (3)$$

where $p_{eq}(x)$ is the equilibrium or stationary distribution for the underlying dynamics of X, $p(x_{i\Delta t} \to x_{(i+1)\Delta t})$ is the short-time transition probability from $x_{i\Delta t}$ to $x_{(i+1)\Delta t}$.

For an exchange between configuration and path space, a new state $z' = \{y', X'(\tau')\}$ is generated from the current

FIG. 1. Schematic representation (a) and pseudocode (b) of the SPEx algorithm.

state $z = \{y, X(\tau)\}$ [Fig. 1(a)]. The new configuration y' is obtained by selecting a point on the current trajectory $X(\tau)$ with probability $p^{\text{sel}}[y'|X(\tau)]$. The generation probability for this move is

$$p_y^{\text{gen}}[X(\tau) \to y'] = p^{\text{sel}}[y'|X(\tau)]. \qquad (4)$$

A new path X' is generated by integrating the equations of motion forward and backward in time starting from y until a stable state is reached. The generation probability for X' is

$$P_X^{\text{gen}}[y \to X'(\tau')] = \prod_{i=k}^{\tau'/\Delta t-1} p(x'_{i\Delta t} \to x'_{(i+1)\Delta t})$$
$$\times \prod_{i=1}^{k} \bar{p}(x'_{i\Delta t} \to x'_{(i-1)\Delta t}), \qquad (5)$$

where $k\Delta t$ is the time of the shooting point on the new path. Since the transition probability fulfills microscopic reversibility, the above distribution can be written as

$$P_X^{\text{gen}}[y \to X'(\tau')] = \frac{1}{p_{\text{eq}}(y)} \times P_X[X'(\tau')]. \qquad (6)$$

Imposing detailed balance, the acceptance probability for the exchange move must obey

$$\frac{P_z^{\text{acc}}(z \to z')}{P_z^{\text{acc}}(z' \to z)} = \frac{P_z(z')P_z^{\text{gen}}(z' \to z)}{P_z(z)P_z^{\text{gen}}(z \to z')}, \qquad (7)$$

which can be satisfied using the Metropolis rule,

$$P_z^{\text{acc}}(z \to z') = \min\left\{1, \frac{P_z(z')P_z^{\text{gen}}(z' \to z)}{P_z(z)P_z^{\text{gen}}(z \to z')}\right\}. \qquad (8)$$

Inserting expressions from Eqs. (1), (4), and (6) finally yields

$$P_z^{\text{acc}}(z \to z') = H_{\text{AB}}[X'(\tau')]$$
$$\times \min\left\{1, \frac{p_y(y')}{p_y(y)} \frac{p_{\text{eq}}(y)}{p_{\text{eq}}(y')} \frac{p^{\text{sel}}[y|X'(\tau')]}{p^{\text{sel}}[y'|X(\tau)]}\right\}. \qquad (9)$$

The exchange scheme is most efficient if $p_y(y)$ has significant overlap with $p_{\text{eq}}(y)$ and shooting moves starting from configurations y have a reasonable probability of generating a transition path. Both conditions can be matched by setting the distribution $p_y(y)$ to the Boltzmann distribution with a time-dependent bias potential introduced via well-tempered metadynamics [6,7]:

$$p_y(y, \hat{t}) = Z(\hat{t})^{-1} \exp\{-\beta[U(y) + U_{\text{bias}}(r(y), \hat{t})]\}, \qquad (10)$$

where $\hat{t}$ denotes the metadynamics simulation time. The acceptance of the exchange scheme can be further improved by tuning the selection probability $p^{\text{sel}}[y'|X(\tau)]$. We can bias this selection in the spirit of Jung et al. [20] according to the current bias introduced by metadynamics,

$$p^{\text{sel}}[y'|X(\tau)] = \frac{\exp\{-\beta[U_{\text{bias}}(r(y'), \hat{t})]\}}{\sum_{i=0}^{\tau/\Delta t} \exp\{-\beta[U_{\text{bias}}(r(x_{i\Delta t}), \hat{t})]\}}. \qquad (11)$$

The acceptance probability for the exchange then becomes

$$P_z^{\text{acc}}(z \to z') = H_{\text{AB}}[X'(\tau')]$$
$$\times \min\left\{1, \frac{\sum_{i=0}^{\tau/\Delta t} \exp\{-\beta[U_{\text{bias}}(r(x_{i\Delta t}), \hat{t})]\}}{\sum_{i=0}^{\tau'/\Delta t} \exp\{-\beta[U_{\text{bias}}(r(x'_{i\Delta t}), \hat{t})]\}}\right\}. \qquad (12)$$

The resulting criterion therefore represents the ratio of the times the old and new paths spend in regions with a high bias potential. This expression is very similar to the reweighting factor necessary when initiating paths from a biased distribution of shooting points [14]. During the exchange, y acts as a shooting point to generate X' and y', selected on X, is chosen with the same procedure as a shooting point in regular TPS. Therefore, we call the exchange scheme *shooting point exchange* (SPEx). A pseudocode for the algorithm is provided in Fig. 1(b).

We first test SPEx on a double well model [Figs. 2(a) and 2(b)]. In this system, two factors complicate the efficient sampling of configuration and path space: Not only does a barrier separate the stable states, but also the reaction channels connecting them. Hence, sampled transition paths show correlations since subsequently sampled paths tend to
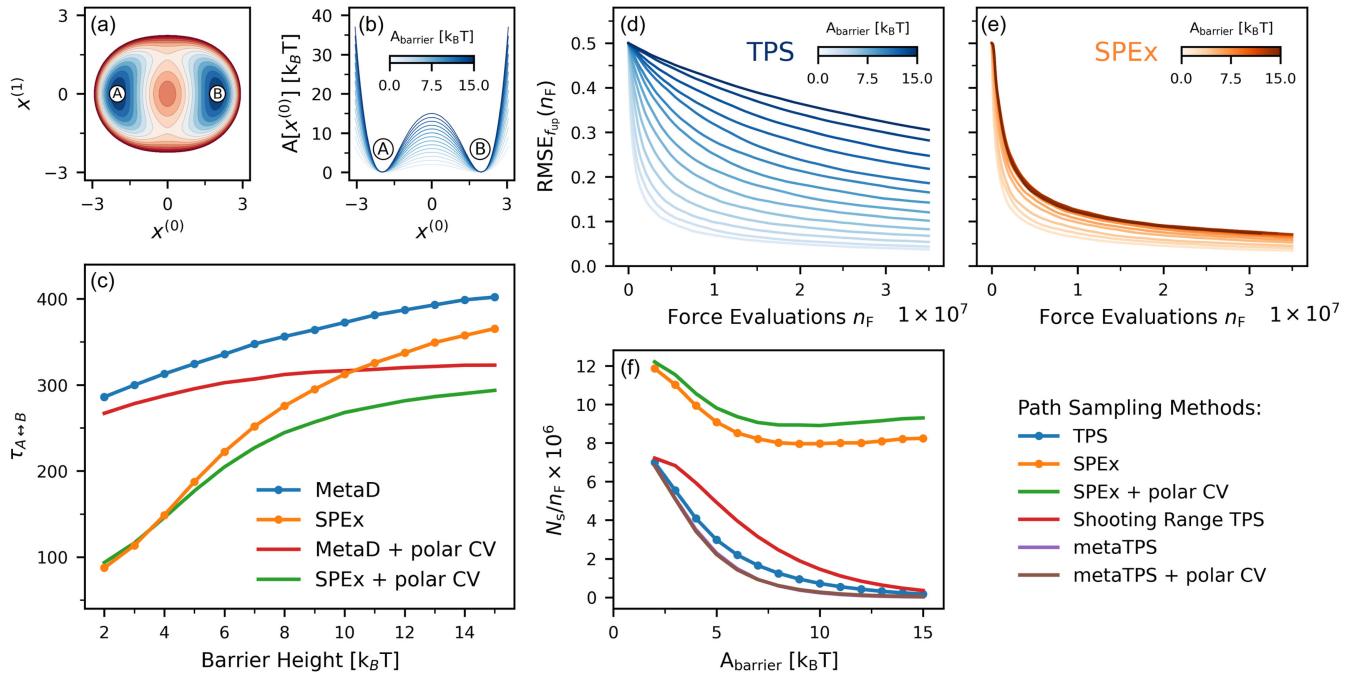
FIG. 2. Shooting point exchange for sampling the two reaction channels in a two-dimensional double well model. (a) Potential energy and state definitions of the model system. (b) Free energy as a function of $x^{(0)}$ for different barrier heights. (c) Average switching time between states A and B, $\tau_{A\leftrightarrow B}$, for stand-alone metadynamics and metadynamics with SPEx, starting the sampling from a converged bias potential. Methods are tested with $x^{(0)}$ and the polar angle (Polar CV) as the reaction coordinate. (d),(e) Root mean squared error of the fraction of paths in the upper reaction channel as a function of simulation length for standalone TPS and SPEx. Each curve is for a specific barrier height and is estimated from 2500 independent sampling runs. (f) Number of switches between the upper and lower reaction channel N_s per force evaluation n_F as a function of the barrier height for different path sampling methods.

remain in the same reaction channel. We compare the performance of stand-alone metadynamics and TPS with the performance of SPEx for different barrier heights and for two different collective variables (simulation details are provided in the Supplemental Material [21]). In configuration space, sampled with metadynamics, we measure the time needed to switch between stable states A and B, $\tau_{A\leftrightarrow B}$. The exchange moves reduce the switching time between the two states for all barrier heights [Fig. 2(c)]. As the speedup is linked to the number of accepted exchanges, the effect is more pronounced at smaller barrier heights due to an increased likelihood of generating a transition path from configurations away from the barrier.

A limiting factor for the sampling of transition pathways is the slow switching between the upper and lower reaction channel. In regular TPS, shooting range TPS [20] and metaTPS [12], the fraction of paths taking the upper reaction channel converges very slowly to the fraction $f_{\mathrm{up}} = \frac{1}{2}$. This is apparent looking at the root mean square error (RMSE) of f_{up} as a function of the trial number n estimated from N runs [Figs. 2(d) and 2(e)]:

$$\mathrm{RMSE}_{f_{\mathrm{up}}}(n) = \sqrt{\sum_{i=0}^{N} \left(f_{\mathrm{up}}(n) - \frac{1}{2} \right)^2}. \qquad (13)$$

In comparison, using SPEx speeds up the convergence substantially [Fig. 2(e)], especially for high barriers. This can be traced back to an increased number of switches during the sampling of the path ensemble [Fig. 2(f)]. Above barriers of $10k_{\mathrm{B}}T$, often not even a single switch between the channels occurs within 1×10^6 force evaluations in standard TPS. When exchange moves are included, a minimum number of switches is recovered, mostly mediated by the exchange moves themselves.

From these observations, we conclude that exchanges between an enhanced sampling simulation in configuration space and a path sampling simulation increase the sampling efficiency on both sides compared to running the two simulations separately. While the decreased switching time $\tau_{A\leftrightarrow B}$ is not negligible, the additional cost of sampling a path ensemble in parallel is not compensated. Therefore, at least in this setup, SPEx is not expected to increase the sampling efficiency when the interest is solely on configuration space. In contrast, when sampling path space, the additional force evaluations of metadynamics are insignificant compared to the number of force evaluations needed for path generation. This is due to the fact that, for the systems studied here, configuration space is explored much more quickly than the path ensemble. Therefore, the number of metadynamics steps between exchanges is only a fraction of the average path length.
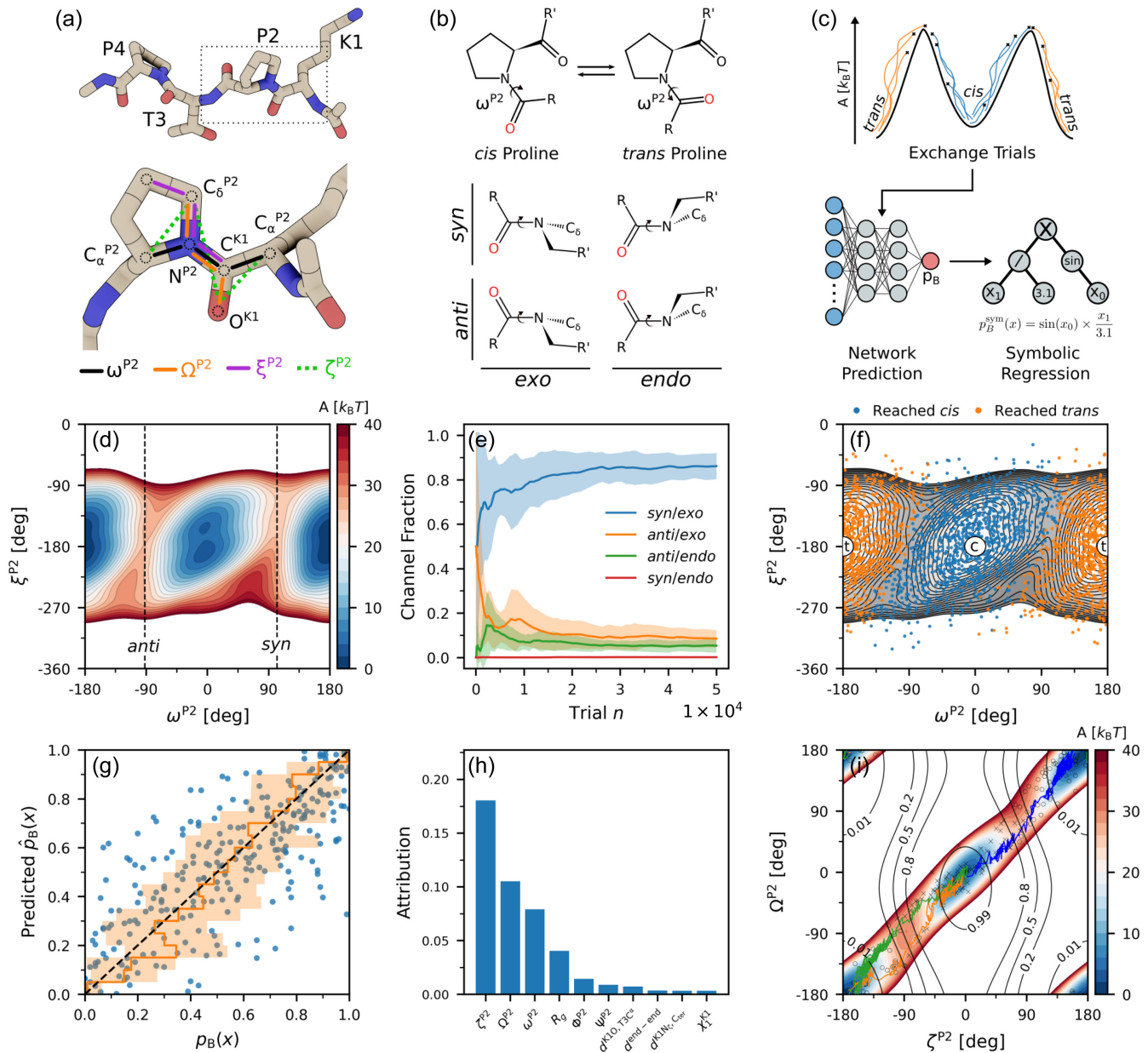
FIG. 3. Isomerization of proline in the tetrapeptide KPTP. (a) Structure of the peptide (relevant torsion angle definitions in the inset). (b) Scheme of the *cis* to *trans* isomerization and the transition state geometry. (c) Schematic overview of the committor learning process. (d) Free energy from metadynamics including shooting point exchanges reconstructed from the converged metadynamics bias potential. (e) Fraction of paths in each reaction channel as a function of the number of trials based on ten independent shooting point exchange simulations. (f) Training data for the committor prediction on top of the free energy surface. Circles show the state definitions ($c = cis$, $t = trans$). (g) Comparison of the sampled committor from fleeting trajectories and the predicted committor. The dashed black line shows the ideal correspondence while the orange line and shaded area show the average and standard deviation of the sampled committor in a given window of the predicted committor. (h) Attributions corresponding to the ten most important input features of the neural network. (i) Free energy along the two most relevant collective variables from (h). Black lines show isolines of the committor function obtained using symbolic regression. Crosses and circles indicate if a trajectory starting from that point reached the *cis* or *trans* state first. Representative reactive paths are shown in the same color scheme as in (e).

As a second case study, we investigate the *cis* to *trans* isomerization of the amino acid proline in the tetrapeptide KPTP [29] [Fig. 3(a)]. Proline isomerization plays an important role in protein folding [30,31] and signaling in cells [32,33], yet it only occurs on the timescale of seconds to minutes [34]. Because of the periodic nature of the relevant imide torsion angle ω^{P2}, the transition from *cis* to *trans* and vice versa can take place via different reaction

channels [Fig. 3(b)]. During the transition from $\pm 180°$ (*trans*) to $0°$ (*cis*), the torsion angle can either cross over a barrier at $-90°$ or $108°$, referred to as *anti* and *syn* conformation [35] [dashed lines in Fig. 3(d)]. Additionally, the imide nitrogen geometry, which is planar in the stable *cis* and *trans* states, is deformed out of plane [35]. By the direction of the deformation indicated by the torsion angle η_{P2}, the transition state can be distinguished as *endo* or *exo*, resulting in a total of four channels. The critical out-of-plane deformation is not captured by ω^{P2} and therefore previous works proposed an improper dihedral ζ_{P2} as reaction coordinate [35,36] [Fig. 3(a)]. Other collective variables discussed for the isomerization are the Ψ_{P2} backbone angle [35–37], the puckering state [38,39] of the ring, and solvent interactions [40].

Previous studies focusing on the mechanism of proline isomerization mainly used biased molecular dynamics to enhance the sampling [29,36–39]. As a result, the dynamics of the system were altered and conclusions on the preferred mechanism and a corresponding reaction coordinate were mostly drawn based on minimum energy paths, with a notable exception being the recent work by Moritsugu *et al.* on the Pin1 enzyme [41]. We aim to identify the preferred isomerization mechanism, find relevant degrees of freedom and refine a reaction coordinate based on the unbiased dynamics of the system (simulation details in Supplemental Material [21]). Besides the imide torsion angle, we choose ξ^{P2} [see Fig. 3(a)] for sampling, as we expect it to capture potential geometric changes of both the imide nitrogen and the sidechain. The resulting free energy from metadynamics with shooting point exchanges agrees with previous studies in terms of the barrier height and difference between the *cis* and *trans* state [29,37] [Fig. 3(d)]. However, estimating the different statistical weights of the four reaction channels is not possible. The *endo* and *exo* paths are not discriminated by ξ^{P2} and, more importantly, an estimation based on barrier heights does not account for entropy in path space. Here, the sampled transition paths can give an accurate estimate of the fraction of paths going through each channel [Fig. 3(e)]. These are *syn/exo* 0.862, *anti/exo* 0.084, *anti/endo* 0.053, and *syn/endo* 0.001, pointing out a clear preference for the *syn/exo* pathway.

To find an improved reaction coordinate for the transition, we train a neural network to predict the committor probability $p_B(x)$ of a given configuration as proposed by Jung *et al.* [42]. The committor is the likelihood of reaching state B before state A starting from x and thereby describes the progress of a reaction. From a broad set of collective variables based on which the network predicts the committor, the most important features can be determined by assigning an attribution score [42]. In the context of SPEx, we train the network using the information obtained from exchange moves [Fig. 3(f), network details in Supplemental Material [21]]. Although the training data only contain

labels indicating if *cis* or *trans* was reached first, the network learns to interpolate in ambiguous regions [Fig. 3(g)]. Looking at the assigned attributions [Fig. 3(h)], the torsion angles ζ^{P2}, Ω^{P2}, and ω^{P2} are the most important variables, followed by the radius of gyration R_g, which has been discussed to be linked to the fraction of *cis* proline residues [29]. Collective variables describing the puckering state of the ring, Ψ_{P2}, and all other backbone angles do not contribute significantly to the prediction of the committor. The neural network prediction is then used to refine an expression for a reaction coordinate via symbolic regression. We only include the three torsion angles in the analysis to obtain a reaction coordinate independent of the peptide sequence.

The most accurate estimate of $p_B(x)$ from symbolic regression includes ζ^{P2} and Ω^{P2} [Fig. 3(i)]:

$$p_B(\zeta^{P2}, \Omega^{P2}) = \text{sig}\big[-\sin(\Omega^{P2} - 0.75) + 4.334\cos(\zeta^{P2}) + \cos(\Omega^{P2}) - 0.635\big], \tag{14}$$

where $\text{sig}(x) = 1/[1 + \exp(-x)]$. Although ζ^{P2} is a better reaction coordinate than ω^{P2} as shown in previous works, the committor isolines indicate that at least Ω^{P2} is required for an accurate prediction of $p_B(x)$. Additional simulations of the KPTP system using standard TPS and with equation (14) as bias coordinate as well as simulations of trp-cage folding can be found in the Supplemental Material [21]. From these simulations it is evident that the time dependence of the metadynamics simulation may impact the performance in complex systems with slow dynamics or with a suboptimal reaction coordinate. To address these issues, iterative reaction coordinate refinement or combinations of SPEx with different biasing methods should be considered in future works.

To conclude, we presented a simulation framework based on exchange moves between a configuration and a path ensemble. The sampling scheme has the potential to efficiently explore free energy surfaces, transition path ensembles and reaction coordinates of molecular processes, as demonstrated on the proline *cis-trans* isomerization. The case studies presented here—combining metadynamics and TPS—are just one realization of the possibilities emerging from Eq. (9). Since the generalized ensemble is not limited to specific configuration and path ensembles, we see future applications, e.g., in umbrella sampling [8], multistate TPS [43], or TIS [44].

The data that support the findings of this study are available upon reasonable request.

*christoph.dellago@univie.ac.at

[1] Arjun, T. A. Berendsen, and P. G. Bolhuis, Proc. Natl. Acad. Sci. U.S.A. **116,** 19305 (2019).

[2] G. Menzl and C. Dellago, J. Chem. Phys. **145,** 211918 (2016).

[3] C. Leitold, C. J. Mundy, M. D. Baer, G. K. Schenter, and B. Peters, J. Chem. Phys. **153,** 024103 (2020).

[4] J. Juraszek and P. G. Bolhuis, Proc. Natl. Acad. Sci. U.S.A. **103,** 15859 (2006).

[5] K. ichi Okazaki, D. Wöhlert, J. Warnau, H. Jung, Özkan Yildiz, W. Kühlbrandt, and G. Hummer, Nat. Commun. **10,** 1742 (2019).

[6] A. Laio and M. Parrinello, Proc. Natl. Acad. Sci. U.S.A. **99,** 12562 (2002).

[7] A. Barducci, G. Bussi, and M. Parrinello, Phys. Rev. Lett. **100,** 020603 (2008).

[8] G. Torrie and J. Valleau, J. Comput. Phys. **23,** 187 (1977).

[9] C. Dellago, P. G. Bolhuis, F. S. Csajka, and D. Chandler, J. Chem. Phys. **108,** 1964 (1998).

[10] P. G. Bolhuis, D. Chandler, C. Dellago, and P. L. Geissler, Annu. Rev. Phys. Chem. **53,** 291 (2002).

[11] P. G. Bolhuis and G. Csányi, Phys. Rev. Lett. **120,** 250601 (2018).

[12] E. Borrero and C. Dellago, Eur. Phys. J. Spec. Top. **225,** 1609 (2016).

[13] D. Mandelli, B. Hirshberg, and M. Parrinello, Phys. Rev. Lett. **125,** 026001 (2020).

[14] S. Falkner, A. Coretti, S. Romano, P. L. Geissler, and C. Dellago, Mach. Learn. **4,** 035050 (2023).

[15] G. Hummer, J. Chem. Phys. **120,** 516 (2004).

[16] R. H. Swendsen and J.-S. Wang, Phys. Rev. Lett. **57,** 2607 (1986).

[17] Y. Sugita and Y. Okamoto, Chem. Phys. Lett. **314,** 141 (1999).

[18] T. S. van Erp, Phys. Rev. Lett. **98,** 268301 (2007).

[19] A. Gil-Ley and G. Bussi, J. Chem. Theory Comput. **11,** 1077 (2015).

[20] H. Jung, K. ichi Okazaki, and G. Hummer, J. Chem. Phys. **147,** 152716 (2017).

[21] See Supplemental Material at http://link.aps.org/supplemental/10.1103/PhysRevLett.132.128001 for simulation and network details. The document contains Refs. [22–28].

[22] N. Goga, A. J. Rzepiela, A. H. de Vries, S. J. Marrink, and H. J. C. Berendsen, J. Chem. Theory Comput. **8,** 3637 (2012).

[23] W. L. Jorgensen, J. Chandrasekhar, J. D. Madura, R. W. Impey, and M. L. Klein, J. Chem. Phys. **79,** 926 (1983).

[24] P. Eastman, J. Swails, J. D. Chodera, R. T. McGibbon, Y. Zhao, K. A. Beauchamp, L.-P. Wang, A. C. Simmonett, M. P. Harrigan, C. D. Stern, R. P. Wiewiora, B. R. Brooks, and V. S. Pande, PLoS Comput. Biol. **13,** e1005659 (2017).

[25] M. Bonomi et al., Nat. Methods **16,** 670 (2019).

[26] D. A. Sivak, J. D. Chodera, and G. E. Crooks, J. Phys. Chem. B **118,** 6466 (2014).

[27] R. B. Best, G. Hummer, and W. A. Eaton, Proc. Natl. Acad. Sci. U.S.A. **110,** 17874 (2013).

[28] M. Huang, T. J. Giese, T.-S. Lee, and D. M. York, J. Chem. Theory Comput. **10,** 1538 (2014).

[29] J. Alcantara, R. Stix, K. Huang, A. Connor, R. East, V. Jaramillo-Martinez, E. J. Stollar, and K. A. Ball, Front. Mol. Biosci. **8,** 734169 (2021).

[30] W. J. Wedemeyer, E. Welker, and H. A. Scheraga, Biochemistry **41,** 14637 (2002).

[31] F. Favretto, D. Flores, J. D. Baker, T. Strohäker, L. B. Andreas, L. J. Blair, S. Becker, and M. Zweckstetter, Nat. Commun. **11,** 6046 (2020).

[32] K. P. Lu, G. Finn, T. H. Lee, and L. K. Nicholson, Nat. Chem. Biol. **3,** 619 (2007).

[33] P. Sarkar, C. Reichman, T. Saleh, R. B. Birge, and C. G. Kalodimos, Mol. Cell **25,** 413 (2007).

[34] C. Grathwohl and K. Wüthrich, Biopolymers **20,** 2623 (1981).

[35] S. Fischer, R. L. Dunbrack, and M. Karplus, J. Am. Chem. Soc. **116,** 11931 (1994).

[36] C. Melis, G. Bussi, S. C. R. Lummis, and C. Molteni, J. Phys. Chem. B **113,** 12148 (2009).

[37] G. P. D. Martino, M. Masetti, A. Cavalli, and M. Recanatini, Proteins **82,** 2943 (2014).

[38] Y. K. Kang and H. Y. Choi, Biophys. Chem. **111,** 135 (2004).

[39] D. Wu, AIP Adv. **3,** 032141 (2013).

[40] H. Ke, D. Mayrose, and W. Cao, Proc. Natl. Acad. Sci. U.S.A. **90,** 3324 (1993).

[41] K. Moritsugu, N. Yamamoto, Y. Yonezawa, S.ichi Tate, and H. Fujisaki, J. Chem. Theory Comput. **17,** 2522 (2021).

[42] H. Jung, R. Covino, A. Arjun, P. G. Bolhuis, and G. Hummer, Nat. Comput. Sci. **3,** 334 (2023).

[43] J. Rogal and P. G. Bolhuis, J. Chem. Phys. **129,** 224107 (2008).

[44] T. S. van Erp, D. Moroni, and P. G. Bolhuis, J. Chem. Phys. **118,** 7762 (2003).